

Review

Active Sites in Heterogeneous Catalytic Reaction on Metal and Metal Oxide: Theory and Practice

Yanbo Pan , Xiaochen Shen , Libo Yao, Abdulaziz Bentalib and Zhenmeng Peng *

Department of Chemical and Biomolecular Engineering, The University of Akron, Akron, OH 44325, USA; yp22@zips.uakron.edu (Y.P.); xs14@zips.uakron.edu (X.S.); lly7@zips.uakron.edu (L.Y.); asb104@zips.uakron.edu (A.B.)

* Correspondence: zpeng@uakron.edu; Tel.: +1-330-972-5810

Received: 29 August 2018; Accepted: 16 October 2018; Published: 20 October 2018



Abstract: Active sites play an essential role in heterogeneous catalysis and largely determine the reaction properties. Yet identification and study of the active sites remain challenging owing to their dynamic behaviors during catalysis process and issues with current characterization techniques. This article provides a short review of research progresses in active sites of metal and metal oxide catalysts, which covers the past achievements, current research status, and perspectives in this research field. In particular, the concepts and theories of active sites are introduced. Major experimental and computational approaches that are used in active site study are summarized, with their applications and limitations being discussed. An outlook of future research direction in both experimental and computational catalysis research is provided.

Keywords: heterogeneous catalysis; active sites; characterization techniques; computational approach; DFT

1. Introduction

A catalyst by definition is a material that mediates the reaction pathway of a chemical process without itself being expended [1]. Distinguished by whether catalyst material and reacting species are in a same or different phase, a catalytic process can be classified as homogeneous catalysis or heterogeneous catalysis. This review article put the focus on heterogeneous catalysis and catalyst materials, which have vast applications in different areas. Thousands of products demanded by modern society like gasoline, tires, cloth, drugs, and polymers would not be possible without catalytic production processes. Catalysts also play an essential role in environmental control such as water and air pollution treatment and in energy applications such as fuel cells and metal-air batteries.

The study of heterogeneous catalysis could be dated back to the 1800s. Faraday was one of the first scientists who examined the ability of platinum to facilitate oxidation reactions [2]. Until now, heterogeneous catalysis is crucial to chemical technology, with a large variety of catalyst materials being developed and widely used in important industrial processes such as ammonia synthesis [3–5], water-gas shift reaction [6,7], methane reforming [8–10], and CO₂ hydrogenation [11–14]. The catalysts are primarily metal and metal oxide-based materials, which normally take the form of nanoparticles with large specific surface area [15]. For instance, gold nanoparticles supported on reducible oxides were found to be active for CO oxidation to CO₂ under ambient condition due to a quantum size effect which is related to the thickness of Au islands, which could be utilized for CO level reduction in buildings by formulating Au/TiO₂ nanopowders with paint that covers the interior wall [16]. With surface Au atoms being considered as active sites, the CO oxidation properties can be affected by certain catalyst material parameters like Au particle size and structure, reducible oxide type, and state. Vanadium oxide nanoparticles supported on metal oxides like ZrO₂, Al₂O₃, and MgO were found

to be active in oxidative dehydrogenation of alkanes to olefins due to the stoichiometric reduction cycle of vanadium oxide following the Mars-van-Krevelen (MvK) mechanism, with the activity and coking resistance properties being alterable by the vanadium oxide particle size [17,18]. These findings revealed complexity of the active sites in catalyzing the reactions and the properties of active sites could be influenced by many material parameters. Hence, in order to understand heterogeneous catalysis and realize fine control of the reaction properties, insightful knowledge of active sites, including the structure, chemical status, and interactions with both reactant molecules and substrate materials, is essential.

This review aims at providing a glimpse of the active site studies, which is divided into three sections including the past achievements, current status and challenges, and an outlook into the future research. Both experimental studies and computational simulations of the active sites are reviewed, with catalysts being mainly focused on metal and metal oxide-based materials.

2. Past Achievements

2.1. Concept and Theory of Active Sites

The concept of active sites in heterogeneous catalysis was firstly introduced by Tylor in 1925 [19]. He suggested that only a small fraction of catalyst surface (active sites or centers), which might be composed of an atom or an ensemble of atoms situated at surface defects such as corners, edges, and other crystalline discontinuities, is catalytically active. The idea that the number of active sites is significantly smaller than the total available surface sites was supported by the fact that the amount of poisoning species being required to effectively deactivate a catalyst was often much less than a monolayer coverage of the catalyst surface. This led to the definition of Taylor Ratio (TR) which describes the fraction of active sites out of the total number of catalyst surface sites [20]. In the same period of time, Balandin [21,22] proposed a multiplet theory, suggesting that reacting species could be simultaneously adsorbed to a group of active atoms of catalyst to form a multiplet complex. He also introduced the correspondence between the geometry of active center and the energies of forming and breaking chemical bonds.

Proceeding with Taylor's principle of the existence of active sites on catalyst surfaces, Boudart et al. classified reactions in terms of whether they are catalyst surface sensitive or not [23]. The reaction rate of a surface-insensitive process would not change with the exposed planes of a single crystal or the size of particles, whereas that of a surface-sensitive reaction would change significantly. Ethylene hydrogenation catalyzed by platinum is considered as one good example of a surface-insensitive reaction. There have been previous studies over a wide range of dispersions of Pt nanoparticles, as well as single crystals and poly-crystals showing little effects on the reaction rate [20,24,25], suggesting all surface Pt atoms are active sites and behave similarly, regardless of their crystallographic planes and locations. On the other side, many other hydrocarbon conversion reactions have also been reported to be surface sensitive [26–28]. Figure 1 shows the structure sensitivity in alkane isomerization reactions catalyzed over platinum single-crystal surfaces [28], which correlates the activity and crystal planes as well as surface atomic ensembles. The results suggest that square surface atom ensembles rather than hexagonal ones favor alkane aromatization and isomerization reactions. One most prominent example of surface-sensitive reaction is ammonia synthesis using iron catalyst. The determined activity ratio of Fe(111):Fe(100):Fe(110) at 798 K was reported to be 418:25:1, suggesting that Fe(111) plane was the most active in this reaction [5]. The development of surface science approach, utilizing structurally and compositionally well-defined surfaces to examine individual reaction steps and intermediates under ultra-high vacuum complement to single crystal studies further advanced the understanding of surface structure dependence [29]. For instance, Somorjai et al. applied surface science techniques to study the enhanced reaction activity of step sites compared to close-packed surface sites [30,31]. The surface structure sensitivity in catalysis has also been correlated with the electronic structure that would be altered with surface structure and influence the catalytic properties. One example is the

electronic band structure of transition metals, which would be altered when the size is reduced from crystallites to nanoscale that results in different physiochemical and catalysis properties compared with the corresponding bulk ones [32].

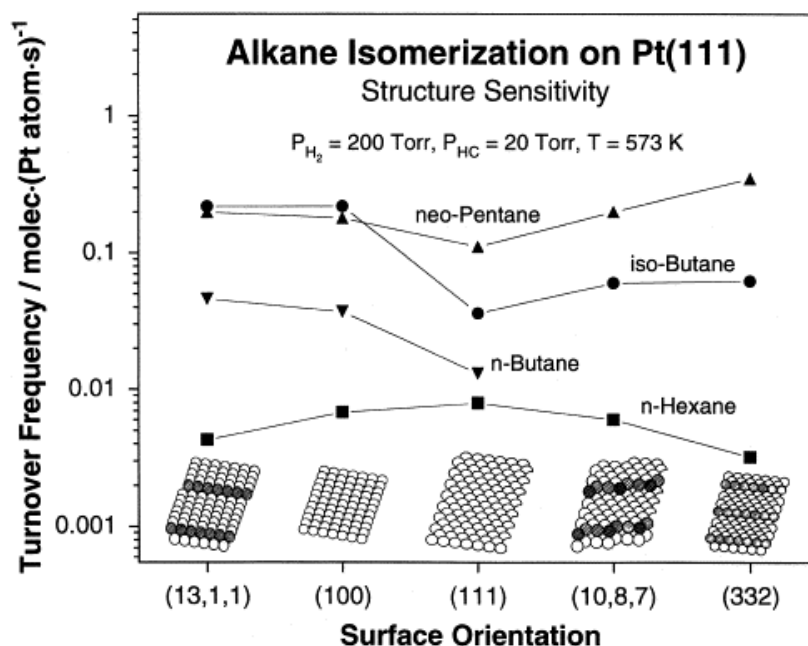


Figure 1. Structure sensitivity in alkane isomerization reactions catalyzed over platinum single-crystal surfaces. Adapted with permission from [28], Elsevier, 2001.

It is generally accepted nowadays that the active sites have two primary catalytic functions, that is, promoting the reaction kinetics and controlling the product selectivity [33]. The active sites would reduce the potential energy barrier or activation energy in the reaction paths by temporarily forming moderate chemical bonds with the adsorbing molecules so that the residence time of the adsorbates is long enough for the chemical rearrangement to occur. Either too strong or too weak bonding between the active sites and the reacting species would lead to a poor catalytic performance. When the active site-reacting species interactions are too strong, the reaction species will strongly adsorb to the active sites that results in permanent blocking of the sites and thus catalyst poisoning. On the other side, too weak interactions would not be able to help break the intramolecular bonds (like H-H, C-H, C-C, C=O and N=N bonds within reactant molecules and requiring activation for reaction) of the reactant [33]. The other important function of active sites is to control the reaction product selectivity. A good catalyst would facilitate the generation of only desired product molecules by suppressing side reaction pathways. To achieve these two catalytic functions, a good understanding of active sites and the interactions with reacting species, which would guide catalyst development with active sites of desired features, is essential.

Three major catalysis mechanisms have been discovered [34], namely the Langmuir-Hinshelwood (L-H) mechanism in which two reacting species simultaneously adsorb to active sites and react with each other, the Eley-Rideal (E-R) mechanism in which adsorbed species reacts with bulk phase molecules, and the Mars-van-Krevelen (MvK) mechanism in which one reactant bonds to the active sites and the other reacting species is provided from local defect sites on support that would be replenished upon consumption by reaction with bulk phase molecules [35]. A vast majority of catalytic reactions have been reported to follow the L-H mechanism. One prominent example is CO oxidation on Pt, in which adsorbed CO reacts with adsorbed oxygen on Pt surface sites [36]. Because the CO adsorption to Pt is too strong that leads to a high CO surface coverage, it largely prohibits dissociative O₂ adsorption and consequently the reaction activity, especially at low temperature [37]. In practice,

metals and alloys serve as one important category of heterogeneous catalysts and are active in many reactions, for instance CO₂ reforming of methane [38–42], hydrogenation of aromatics [43], and CO preferential oxidation (PROX) [44,45]. Alloy catalysts were often found to be more active and selective compared to the pure metal counterparts, which could be largely attributed to the ability of electronic and geometry optimization of the active sites with the additional composition parameter knob. For instance, Pt alloy catalysts have attracted considerable attraction due to the much improved activity and selectivity properties than pure Pt in CO oxidation and PROX [46,47]. Based on current understanding [44,48,49], CO PROX on Pt alloy (Pt-M) can be illustrated in Figure 2, with CO oxidation following the dual-site L-H mechanism and H₂ oxidation following the E-L mechanism. To be more specific, CO and O₂ follow a non-competitive adsorption mechanism, with CO adsorbing to Pt site and O₂ dissociatively adsorbing to M site followed by interaction and surface reaction between the adsorbed species to generate CO₂. In this way, O₂ can be activated effectively even at low temperature and the CO oxidation kinetics can thus be dramatically improved compared with that using Pt, on which O₂ cannot be effectively adsorbed and activated at low temperature due to the competitive adsorption with CO. H₂ oxidation at low temperature has to follow the E-L mechanism, in which H₂ in the gas phase reacts directly with adsorbed oxygen at M site, because H₂ undergoes competitive adsorption against CO at Pt site and against oxygen at M site which is typically less electronegative and pre-covered by oxygen. The reported high CO PROX selectivity on Pt-M catalysts, such as Pt-Sn, Pt-Fe, and Pt-Co [50], can be attributed to a relative high activation energy of H₂ oxidation that suppresses the H₂ oxidation at low temperature.

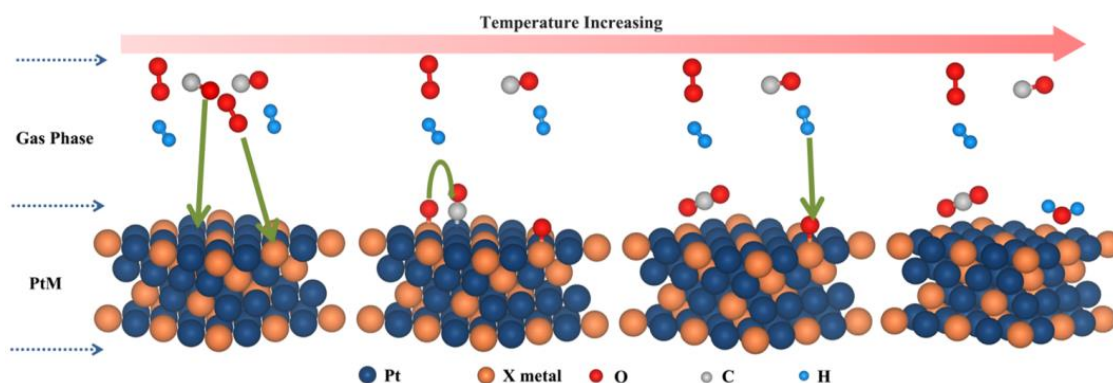


Figure 2. Schematic illustration of CO preferential oxidation (PROX) pathways on Pt-M alloy catalyst. Reprinted with permission from [45], American Chemical Society, 2018.

Another important category of solid materials for heterogeneous catalysis process is acid catalysts, with acid-catalyzed reactions being one of the most studied reaction types for organic functional groups transformations [51]. Various solid catalysts such as zeolites, metal complexes, metal-organic framework (MOF), and zirconia have been reported to be promising candidates in heterogeneous acid catalysis, serving as proton donors to accelerate reaction rates [51–54]. For instance, zeolites (crystalline aluminosilicates interlinked by oxygen atoms) have a three-dimensional framework structure with molecular pores, which makes it possible to exchange ions and produce charges within the framework, while the charges could enhance the catalytic activity [55]. Takahara et al. investigated the performance of zeolites in dehydration of ethanol into ethylene, suggesting that the catalytic activity was directly related to the number of acid sites and the stability could be tuned via the SiO₂/Al₂O₃ ratio [56]. Corma et al. studied the role of different types of acid sites in n-heptane cracking on HY zeolite and found that the cracking process could be initiated on Brønsted acid sites (anions) by protolytic cracking while the cracking on Lewis acid sites (cations) followed the classical β-scission mechanism [57]. Tang et al. prepared nanocrystalline Sn-Beta zeolites by incorporating Sn(IV) into framework of Beta zeolites as a solid Lewis acid catalyst, exhibiting remarkable activity in ring-opening hydration of epoxides under ambient and solvent-free conditions [58]. Other than the

number of acid sites and $\text{SiO}_2/\text{Al}_2\text{O}_3$ ratio, it's believed that the catalytic performance of zeolites is also greatly affected by pore size of zeolites since reactions are mainly restricted within the pores [55]. MOF (a coordination network with organic ligands containing metal ions or clusters) is also widely used as a solid acid catalyst. For instance, Alaerts et al. investigated the acid character of $[\text{Cu}_3(\text{BTC})_2]$ (BTC: benzene-1,3,5-tricarboxylate), which is a zeolite-like porous-framework MOF with Cu(II) ion as the free coordination site, on reactions such as isomerization of α -pinene oxide and the cyclization of citronellal to isopulegol [59]. $[\text{Cu}_3(\text{BTC})_2]$ was identified as a Lewis acid catalyst and was proved to be effective for various acid-catalyzed reactions. Because heterogeneous acid catalysis and homogeneous acid catalysis share similar working mechanism, acid catalyst materials are not focused on in this review.

2.2. Experimental Approach for Studying Active Sites

Identification and study of the active sites where reaction occurs is critical to the catalysis understanding and catalyst development, but demands advanced characterization techniques to investigate the chemical status and structure of catalyst surface atoms at atomic level under the reactive condition. Over the past several decades, multiple techniques have been developed to allow more insightful characterizations of catalyst materials [60].

Surface techniques like low energy electron diffraction (LEED), X-ray photoelectron spectroscopy (XPS), Auger electron spectroscopy (AES), atomic force microscope (AFM), scanning tunneling microscope (STM) and low-energy ion scattering (LEIS) allow direct characterization of the top surface layers of clean solid catalysts and even the adsorbed species, and thus have been widely used in catalyst research [61]. LEED is nowadays one of the most powerful techniques for surface analysis by sending a low energy electron beam (with energies varying from 20 to 500 eV) from an electron gun to samples and collecting the diffracted electrons from the surface of samples as spots on a fluorescent screen [62]. Since low energy electrons are waves and can be diffracted by crystal surfaces, the diffraction patterns can provide information on surface structure and atomic positions. For instance, LEED was applied to study the restructuring of support materials for a Pt-based CO oxidation catalyst and the LEED patterns confirmed that the support (crystalline alumina film) was turned to amorphous after the samples were exposed to CO and O_2 mixture [63]. XPS is a surface technique and one of the standard tools in surface characterization. By exciting core electrons with one soft X-ray beam, XPS could give information on composition and chemical state of the elements on catalyst surface via expulsion and analyses of the related binding energies [64]. Our group applied high-resolution XPS in the study of Pt alloy catalysts and found that Pt atoms on and near the particle surfaces were mainly in the metallic state, while negative shifts in the Pt peak positions comparing to pure Pt indicated electronic interactions of Pt and other metal elements [65]. AES is used to provide information of quantitative elemental and chemical state of material surface by exciting the samples to emit Auger electrons with a focused electron beam and analyzing the kinetic energy of Auger electrons [66]. For instance, Yan et al. applied AES to determine surface composition (Fe/Au ratio) and carbon deposition of $\text{Fe}_2\text{O}_3/\text{Au}(111)$ catalyst in CO oxidation [67]. STM is accomplished by scanning a sharp metal tip very close to sample surface and applying an electrical voltage between the tip and sample, where electrons can tunnel through based on the quantum tunneling effect. The tunneling current is related to position of the tip and local density of states of the sample, which enables build-up of 3D images of the surface with atomic-scale resolution based on the current change [68]. For instance, in the study of gas phase oxidation of benzyl alcohol over $\text{FeO}/\text{Pt}(111)$ (FeO islands on Pt(111) surface), STM was used to investigate the role of interfacial sites. The STM images clearly exhibited a larger density and lower height of adsorbate on the interfacial sites, suggesting that the metal/oxide interfacial sites are the active sites [69]. AFM is also one popular technique for surface characterization nowadays. In this technique, a mechanical probe (normally an atomically sharp tip) scans across a surface and the force change between the tip and the surface atoms is determined by recording the deflection of a small spring-like cantilever. Thereby the surface topography can be constructed even down to an atomic resolution. For instance, Ali et al. used AFM to characterize surface morphology and roughness in the

study of Co-doped ZnO films grown on various crystalline substrates in Fischer-Tropsch synthesis and revealed that the Co-ZnO films consisted of well-isolated nano-globules [70]. LEIS is mainly used to study relative positions of atoms in a surface lattice and chemical composition of sample surface by shooting ions (normally ionized noble gas atoms or alkali atoms) to the sample surface and observing positions, velocities, and energies of the scattered ions [71]. For instance, LEIS was applied to determine surface composition and concentration of metal elements in the study of acetone hydrogenation over various Pt-Ru/C catalysts [72].

Besides the surface characterizations, careful characterizations of the overall structure of catalyst materials are also important to help study the active sites, considering the fact that the generation and performance of active sites would be influenced by the beneath lattice atoms and the local environment. A large number of such techniques are available for use, such as X-ray diffraction (XRD), Raman, infrared spectroscopy (IR), ultraviolet-visible spectroscopy (UV-vis), scanning electron microscopy/transmission electron microscopy (SEM/TEM), high-resolution TEM (HRTEM), extended X-ray absorption fine structure (EXAFS), and X-ray absorption near edge structure (XANES). Both Raman and IR are widely-used vibrational spectroscopy methods in active sites study. Raman spectroscopy is mainly used to provide information on molecular vibrations and crystal structures by irradiating the sample with monochromatic light (usually from a laser) and detecting the Raman scattered light as Raman spectrum after the interaction between laser light and molecular vibrations or photons, wherein the fingerprinting characteristics of the Raman spectrum could be used to identify substances and evaluate crystallinity [73]. IR is mainly used to identify particular functional groups in an unknown sample and is accomplished by passing through the sample with a beam of infrared light, which could be absorbed when frequency of the IR is equal to the vibrational frequency of the bonds within the functional groups [74]. For instance, Otake et al. investigated the activity of a vanadium oxide catalyst supported on metal-organic framework (MOF) for selective alcohol oxidation and used both Raman and IR to characterize the synthesized catalysts, which exhibited the existence of different V-containing bonds before and after reaction and helped reveal that the dehydrated form of V₂ species on MOF are actually the active sites [75]. While the interaction of molecules with infrared light causes vibrational transitions (as in the case of IR), the UV (200–400 nm) and visible light (400–700 nm) with shorter wavelength but higher energy radiation would cause electronic transitions to molecules, which means that the molecules could adsorb certain wavelength of light that matches the energy difference between the possible excited state and ground state of molecules [76]. By measuring the intensity of light before and after the light passes through the sample, UV-vis spectrometer can be used to determine qualitatively and quantitatively the concentration of ions or organic compounds based on the Beer-Lambert Law [77]. For instance, to investigate the activity and deactivation of small-pore zeolites for methanol-to-olefins process, Goetze et al. applied UV-vis to analyze the formation of hydrocarbon species inside the zeolite crystals [78]. EXAFS and XANES are based on X-ray adsorption spectroscopy (XAS), which is obtained when tunable X-ray are shone on sample and incident and transmitted X-ray energy are recorded. The intensity of transmitted X-ray will drop dramatically when the incident X-ray energy matches the binding energy of an electron within the atoms of a sample, resulting in an adsorption edge. Since the binding energies of electrons for different elements are generally different and correspond to their unique adsorption edges, XAS spectra can be used to identify elements and provide information on the electronic structure of sample [79]. In detail, EXAFS allows determination of near neighbor coordination numbers and interatomic distances, while XANES provides information on energy bandwidth, bond angles, and oxidation state. For instance, Magadzou et al. applied EXAFS/XANES to analyze Au-Cu ion mixtures on TiO₂ in the study of low-temperature water-gas shift reaction. XANES spectra confirmed that Cu exists as ions (Cu⁺/Cu²⁺) before and during the reaction while EXAFS spectra suggested that the interaction between Au and Cu is lower than its bimetallic system [80]. XRD was accomplished by shooting a beam of monochromatic X-ray to sample and collecting the diffraction signals, of which the possible directions are related to size and shape of the unit cell and the intensities mainly depend on atom arrangement in the crystal

structure [81]. For instance, XRD was used to identify crystalline phases of mixed metal oxide supports and Ni-based catalyst in CO₂ methanation on Ni catalysts supported on ternary and quaternary mixed oxide [82]. TEM, HRTEM, and SEM are powerful to obtain morphology, crystallinity, size, structure, facet exposure information of characterized catalyst materials. TEM is accomplished by transmitting a beam of electrons through sample and interact with the electrons within the sample, while SEM is done by scanning the surface of sample with a beam of electrons, generating signals that contains information about the surface topography [83,84]. Figure 3 shows the characterizations of nickel nitride nanosheet catalyst with XRD, SEM, HRTEM, and AFM, which confirmed a hexagonal Ni₃N phase, uniform nanosheet morphology, unique porosity in structure, and about 5–7 unit cells in thickness [85].

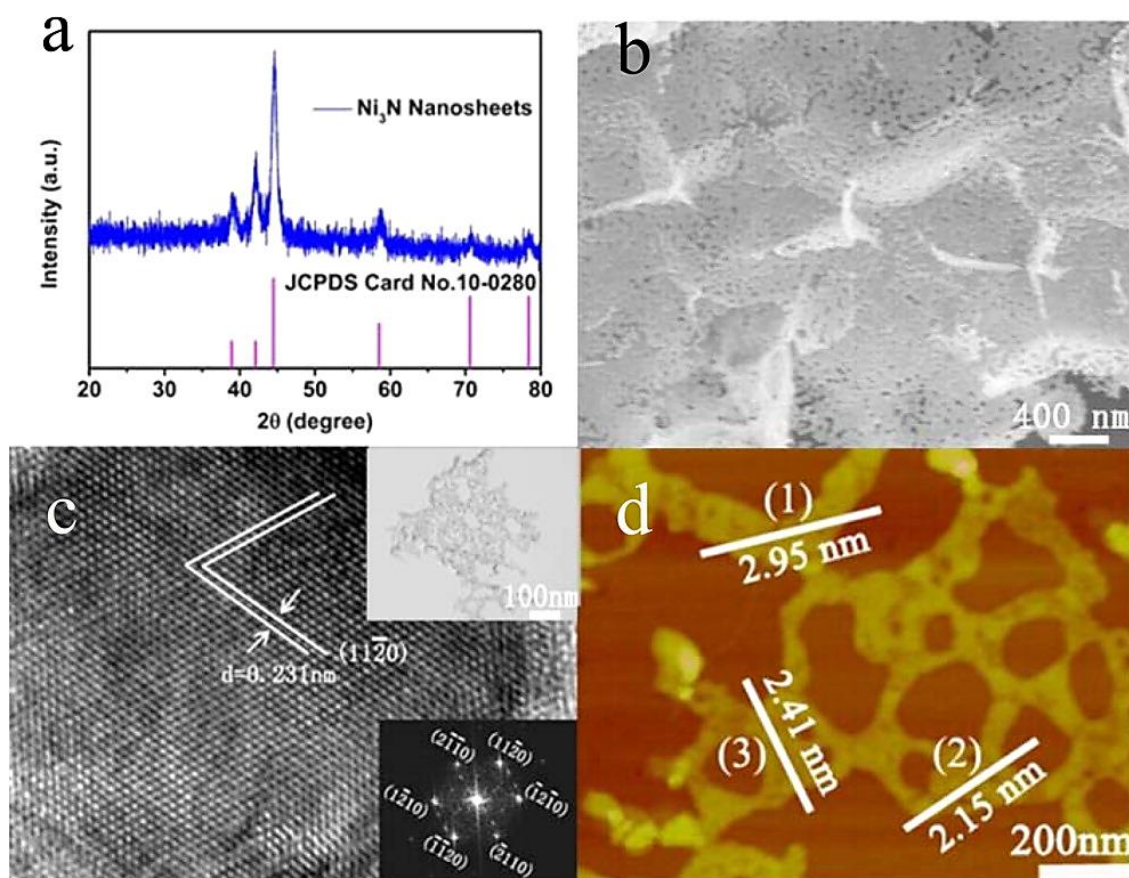


Figure 3. Characterization of Ni₃N nanosheets. (a) XRD pattern; (b) SEM image; (c) HRTEM image. Inset: corresponding FFT pattern and TEM image; (d) AFM image. Reprinted with permission from [85], American Chemical Society, 2015.

2.3. Computational Approach for Studying Active Sites

The computational approach which range from semi-empirical to first principles has become a powerful tool in catalysis study nowadays [86]. The tight-binding method, also known as the Huckel method and one most extensively used semi-empirical method, was initially used to calculate the electronic structures in organic chemistry and later on introduced to study clusters and slabs of transition metal systems [87–89]. This method was further developed by Hoffmann to better model the transition metal systems by specially treating the nonorthogonality of atomic orbits, also known as the EHT method (the extended Huckel method) [90]. EHT considers all valence electrons in a molecular orbital calculation based on the orbital overlaps and experimental ionization potentials and could give reasonable results of the corresponding eigenvalues for the molecular orbitals. However, EHT method also has its limitations when dealing with medium-sized molecules [91]. An extension of the EHT

method was named ASED (atomic superposition and delocalization), in which repulsive interactions were introduced by Anderson and proved to be more reliable in calculating adsorption geometries and energetic trends [92–94]. For instance, Koster et al. studied the adsorption of methyl (CH_3), methylene (CH_2), and methyne (CH) on Rh(111) and Ni(111) with both EHT and ASED method by calculating the local density of states and bond order overlap populations [95]. The results determined the active sites for CH_x species adsorption and showed that the adsorption energy increased with an increase in hydrogen content (x) in CH_x . However, the semi-empirical method has its limitations when dealing with electron-electron interactions and electron correlation, especially for transition metal systems which contains a large number of d-electrons and degenerate eigenstate [96]. Methods such as the ab initio molecular orbital methods and density functional theory (DFT), which are derived from the first principles, have been proven to be effective in the prediction of the electronic and energetic properties in transition metal systems. The most basic approach of ab initio molecular orbital methods is the HF-SCF (Hartree-Fock self-consistent field) method and has been mainly used on small metallic clusters and simple periodic models [97]. The basic concept of HF-SCF method is that one can use a single Slater determinant to approximate the exact N-body wave function of a system and the solution can give us the HF wavefunction and the energy of the system [98]. HF-SCF method is widely used in solving the Schrödinger equation for atoms and nanostructures in active sites study. For instance, Radhakrishnan et al. used HF-SCF calculations to explore the structural possibilities of a $\text{MnO}_x/\text{Al}_2\text{O}_3$ catalyst for ozone decomposition and the calculated vibrational frequencies matched well with the experimental data [99]. However, HF-SCF does not account for the correlations between electrons and sometimes would result in a large deviation from the experimental results.

The development of DFT can be traced back to Thomas and Fermi in the 1920s [100], while it was formally used as one first principle method by Hohenberg and Kohn who demonstrated that the energy is a unique function of the density [101]. With significant advances in the algorithms and methods of DFT as well as the computer power, DFT is now the most widely used computational method in catalysis study and has been able to deal with thousands of atoms with reasonable accuracy. For instance, in the study of identification of the active site of the $\text{Cu}/\text{ZnO}/\text{Al}_2\text{O}_3$ catalyst for industrial methanol synthesis, DFT calculation was conducted to rationalize the effect of the structural features that have been previously identified to be relevant for the catalytic properties, as shown in Figure 4 [102]. The ideal defect-free catalyst was represented by a flat Cu(111) surface while the catalyst with surface defects was represented by a stepped Cu(211) surface (Figure 4 black and blue curves). The CO_2 hydrogenation pathways on the two different surfaces are shown in Figure 4b, being proceeded by forming the intermediates HCOO, HCOOH, and H_2COOH . The C-O bond in H_2COOH was split to generate adsorbed H_2CO and OH, with H_2CO being further hydrogenated to methanol via the methoxy (CH_3O) intermediate. As suggested in Figure 4b, the intermediates were bonded more weakly on the flat Cu(111) than on the stepped Cu(211). In the meantime, the energies of the intermediates and the transition state energies decreased significantly on the (111) surface compared with on the (211) surface, indicating step sites are more active than the terrace sites. The hydrogenation of CO shows similar results (Figure 4c), with a different reaction pathway via the intermediates including HCO, H_2CO , and H_3CO . To study the beneficial role of Zn at the catalyst surface, the Cu(211) surface where Cu in the step was partially substituted by Zn was calculated (Figure 4, red curves). By alloying Zn into the Cu step, the adsorption energies of HCO, H_2CO , and H_3CO did not further increase. However, the energy barriers showed significant decrease, leading to promoted methanol synthesis kinetics. The order of activity for CO_2 and CO hydrogenation is $\text{CuZn}(211) > \text{Cu}(211) > \text{Cu}(111)$. In this way, the active site was suggested to be Cu step site alloyed with Zn.

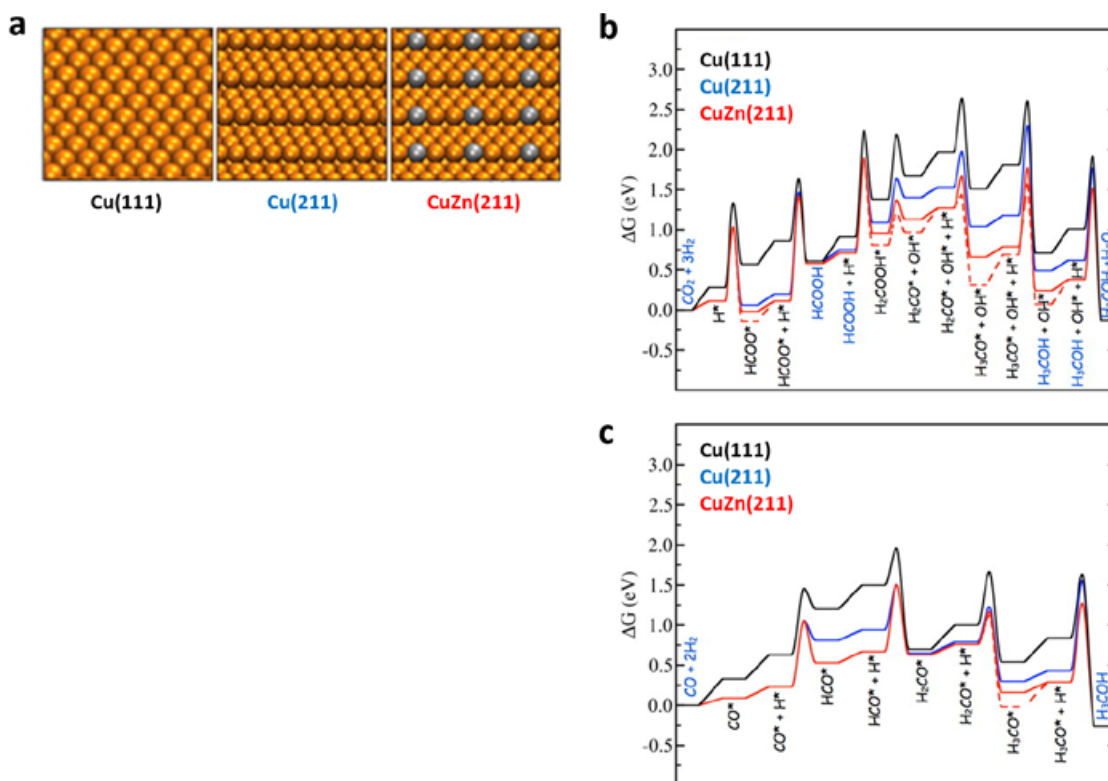


Figure 4. The Cu(111), Cu(211), and CuZn(211) facets as viewed from perspective (a); Gibbs free energy diagram obtained from DFT calculations for CO₂ (b) and CO (c) hydrogenation on close-packed (black), stepped (blue), and Zn substituted steps (red Intermediates marked with a star are adsorbed on the surface. Reprinted with permission from [102], AAAS, 2012.

3. Current Status and Challenges

3.1. Current Status

In recent years, the development of advanced in situ techniques, such as in situ electron microscopy and ambient pressure XPS, enables characterization of active sites under the reactive condition that mimicking the real reaction environment and thus obtaining structural information of the functioning active sites [103–105]. For instance, Vendelbo et al. imaged the oscillatory behavior of Pt nanoparticles during CO oxidation using in situ TEM and revealed that periodic changes in the CO oxidation properties are synchronous with periodic re-faceting of the Pt nanoparticles [106]. Niu et al. reported an in situ study of PbS growth on Au nanorod seeds using liquid cell TEM and observed interfacial dynamics during the Au-PbS core-shell nanostructure formation [107]. Shen et al. in our group combined in situ STEM and operando FTIR techniques to investigate Co(OH)₂-to-CoO transition in 2D nanosheets, as shown in Figure 5 [108]. The STEM images taken under the reaction condition provided clear evidence of intermediate phases that were generated at different transition stages and detailed structural evolution information the at phase boundaries.

The current computational methods have been sufficiently fast to deal with complex systems and accurately provide the interaction energies between molecules and active sites, especially for transition metals and alloys [109,110], which has created the possibility of computer-based activity site identification and design. A combinational use of computation and experiments has made the computational chemistry an even more powerful tool in active sites study. For instance, to design the catalysts based on less expensive and more earth-rich metals for selective hydrogenation of acetylene, DFT calculation was firstly performed on various metals and metal alloys (Figure 6), followed by experiments being conducted to validate the calculation results [111]. Previous studies suggested that the stabilities of adsorbed acetylene and ethylene are two dominant parameters determining

the catalyst activity and selectivity properties and both acetylene and ethylene adsorption energies scale with methyl adsorption energies (Figure 6a) [111]. A good catalyst candidate ideally should have a high stability of adsorbed acetylene, which would promote the acetylene hydrogenation rate, and a low stability of adsorbed ethylene, which would improve the ethylene product selectivity by suppressing its over-hydrogenation. Figure 6a shows that the adsorption energies of acetylene and ethylene, which were linearly correlated that suggests no metals would have weak ethylene adsorption and strong acetylene adsorption in the same time. In other words, there would be certain compromise in the two parameters in catalyst design. This together with the scaling relations (as being discussed in detail in the next section) led to a window of candidate catalyst materials with methyl binding energy as a descriptor parameter (Figure 6a). By calculating the methyl binding energy on about 70 different alloy surfaces, a number of alloy compositions fell into the sight of interest, as shown in Figure 6b, where the constituent cost was plotted versus the methyl adsorption energy. Ni-Zn alloys exhibited particular stability in the analysis of stability of different alloys, and were therefore selected for detailed study. As shown in Figure 6c, the adsorbates are bonded to nickel sites instead of zinc, while the zinc atoms would change the electronic properties of the nickel atoms. A series of Ni-Zn alloy catalysts on MaAl_2O_4 support were synthesized and evaluated for the acetylene hydrogenation properties (Figure 6d). The model Pd-Ag catalyst showed a good selectivity even at high conversion. The Ni-Zn catalyst with 75% zinc content exhibited a comparable selectivity compared with the best Pd-Ag catalyst, which matched well with the DFT calculations.

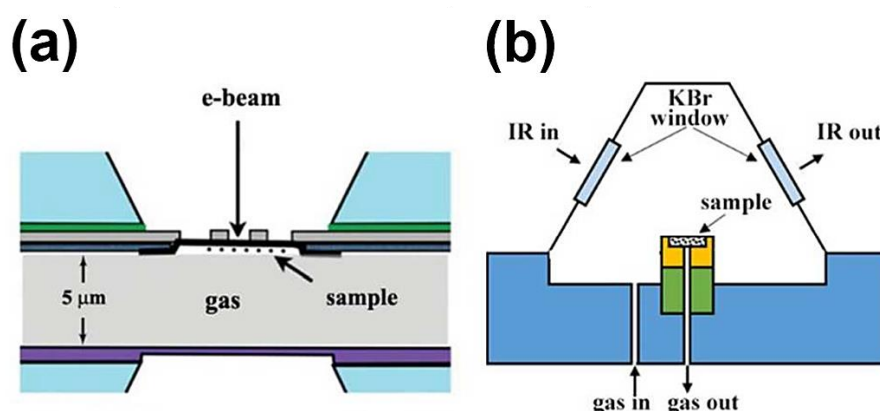


Figure 5. Schematic cross section view of the assembled gas cell with sample loaded for in situ STEM (a) and in situ FTIR (b). Reprinted with permission from [108], American Chemical Society, 2017.

The discovery of scaling relationship is one of the most important findings in computational chemistry in recent years. Previous studies have discovered that the DFT calculation results of a simplified and idealized model could represent the overall catalytic properties of a complexed system to a large extent according to the linear scaling relation. This finding was initially discovered for adsorption on transition metal surfaces [112], and was later on extended to more complex systems such as transition metal carbide [113], oxide [114], and nitride [114] surfaces. According to the scaling relation, the adsorption energies of complex molecules could be estimated from the adsorption energy values of the simple atoms. Luo's group [115] found that the scaling relation also holds nicely at the nanoscale for noble bimetallic particles of different compositions, shapes, and sizes, suggesting that the adsorption energy values calculated from simple atoms could be used to estimate the adsorption energies of alloy nanoparticles with a simple linear scaling relation. The scaling relationship makes it possible to study the active sites in complexed catalytic systems using a simplified model.

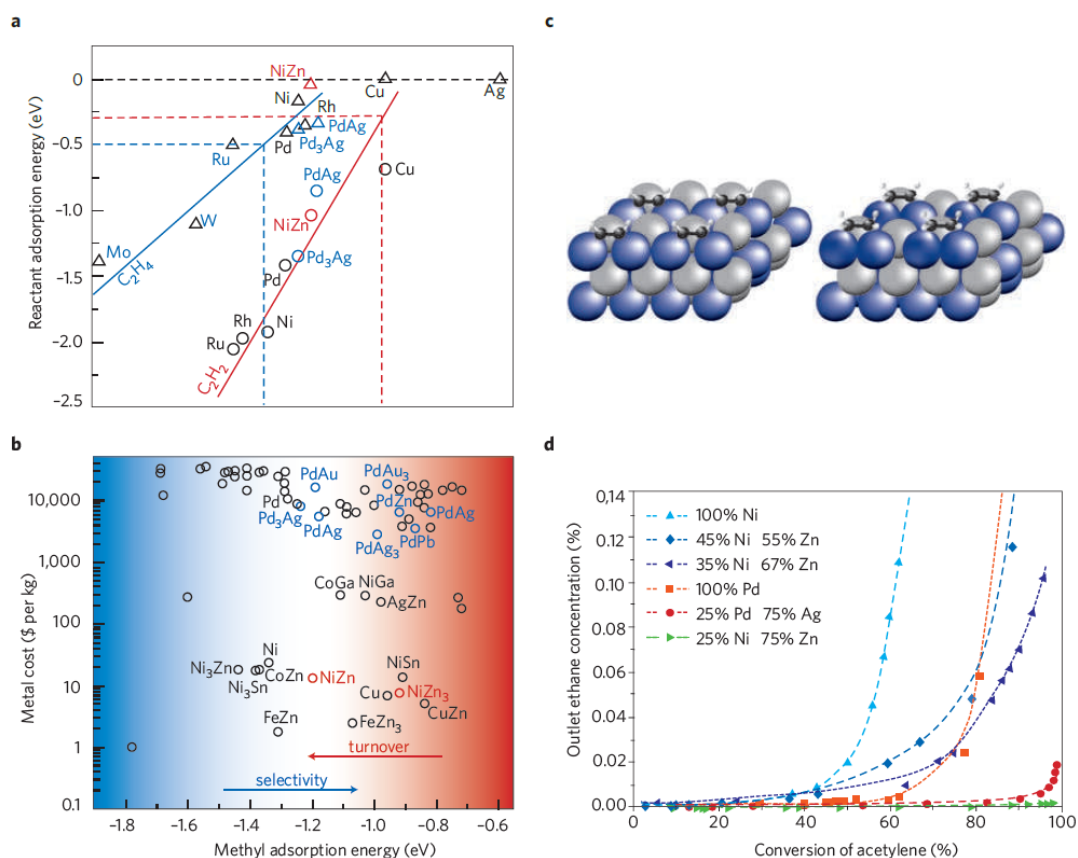


Figure 6. Catalysts design for selective acetylene hydrogenation. **(a)** Heats of adsorption for acetylene (C_2H_2) and ethylene (C_2H_4) plotted against the heat of adsorption for methyl (CH_3). The solid lines show the predicted acetylene (red line) and ethylene (blue line) adsorption energies from scaling. The dotted lines define the region of interest; **(b)** Price (in 2006) of 70 binary intermetallic compounds plotted against the calculated methyl binding energies. The smooth transition between regions of low and high selectivity (blue) and high and low reactivity (red) is indicated; **(c)** Modeling of the NiZn catalyst in the bcc-B2 (110) structure. The Ni atoms are shown as blue and Zn as gray. The adsorption of acetylene (left) and ethylene (right) is shown (small black and white structures); **(d)** Measured concentration of ethane at the reactor outlet as a function of acetylene conversion for seven catalysts. Ethane production is a measure of the selectivity of acetylene hydrogenation, and zero ethane corresponds to the most-selective catalyst. Experimental details are given in the corresponding reference. Adapted with permission from [86], Springer Nature, 2009.

3.2. Present Challenges

It needs to be noted that, although the fast development of advanced characterization techniques and computational chemistry have significantly advanced the study of active sites, there are still technological limitations and challenges associated with these approaches. For instance, the electron microscopy technologies nowadays have been able to characterize surface atoms of catalyst materials at atomic scale. However, the characterizations by themselves are still not conclusive to identify active sites, which can only be proposed as possible ones based on the catalysis mechanisms [116]. Besides, the possible electron beam effects are of concern in influencing the real structure of active sites. Moreover, active sites could be generated in situ under reaction conditions (i.e., the real active sites would be significantly different from ex situ characterized ones). One example is reported in the study of propane metathesis over dispersed molybdenum oxide on silica support. It was found that the active sites were not surface molybdenum oxide but Mo(VI)–alkylidene moieties that were generated under the reaction condition [117]. In some cases, surface rearrangement/restructuring would occur under reaction condition that causes dynamic changes in the active sites. One such

example is VMgO catalyst for oxidative propane dehydrogenation [118], in which a monolayer of amorphous V species were identified as the active sites. These surface V units underwent a reversible order/disorder reconstruction behavior under the reaction condition, which might be attributed to their dynamic redox process during the catalysis cycles.

The use of advanced in situ TEM and STEM characterizations would possibly alter or even damage the active sites due to high-energy electron beams and their interactions with the catalyst materials. How to eliminate the beam effects remains a challenge. A TEM with an operation voltage at 200 kV or more can generate a sub-nanometer electron probe with a current density of about 10^5 A/cm², which could create defects and even destroy the ordering of a crystalline structure, transform amorphous structure to ordered phase, and fluctuate the structure of nanoparticles [116]. For instance, Figure 7 shows the shape and structure of an Au nanoparticle supported on activated carbon under an electron beam [119]. The observed fluctuation in shape and inner structure was attributed to the energy that transfers from the incident electrons to the Au particle.

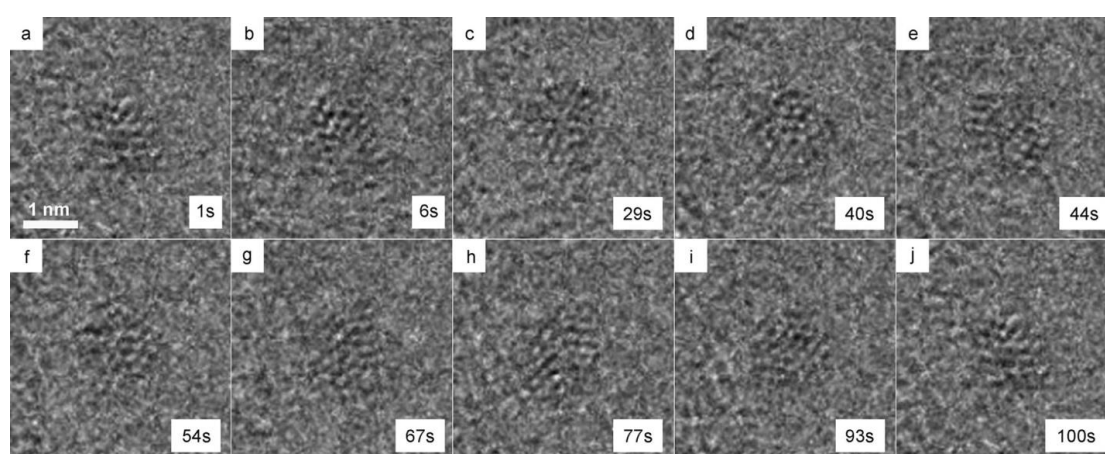


Figure 7. Dynamic changes of a small Au particle supported on activated carbon under electron beam irradiation at various observation times. Electron doses: (a) 1.1×10^6 , (b) 6.6×10^6 , (c) 31.9×10^6 , (d) 44×10^6 , (e) 48.4×10^6 , (f) 59.4×10^6 , (g) 73.7×10^6 , (h) 84.7×10^6 , (i) 102.3×10^6 , (j) 110×10^6 e⁻ nm⁻². Adapted with permission from [119], John Wiley and Sons, 2011.

The electron beam effects would get even more severe when gas and heating are introduced for in situ experiments, because catalyst surface becomes more active when interacting with gas molecules and the heating enhances the frequency and amplitude of atom vibration that result in accelerated electron beam damage [116]. For instance, by exposing V₂O₅ crystallite to an electron beam in liquid helium (4.2 K), Su et al. studied the effect of temperature in electron beam-induced reduction of V₂O₅. They observed that V⁵⁺ was reduced to V⁴⁺ and the structure was transformed from orthorhombic to amorphous phase [120], whereas a similar experiment at room temperature showed that V⁵⁺ was reduced to V²⁺ state with the structure being transferred to stable cubic [121]. The temperature-dependent results indicated that an elevated temperature increased the diffusion rate of oxygen and displaced atoms by the electron beam.

Challenges also await solutions in computational catalysis research. There is always a compromise between computation accuracy and cost in DFT calculations. For instance, DFT calculations could yield estimated kinetic parameters with reasonable accuracy for direct hydrocarbon reactions in combustion, but the computation cost is significantly high [122]. Besides, the selection of approximation to the exchange correlation is important since it greatly affects the accuracy of DFT calculation. However, which approximations should be used for specific systems remains a great issue although the commonly used approximations like local density approximation (LDA) and the generalized gradient approximation (GGA) can handle various many-electrons systems. For instance, Hinuma et al. calculated the energies of different binary oxides with seven different approximations and found that

the strongly constrained and appropriately normed (SCAN) approximations seemed to be the best approximations among all the tested approximations instead of LDA and GGA based on analysis of the calculation results [123]. DFT calculations have been proved to work quite well in many transition metal and metal oxide systems as discussed above. In the meantime, there are still many cases that the DFT cannot handle successfully [124–126]. One example case is DFT simulation of the hybrid organic-inorganic halide perovskite system in the study of photovoltaics for energy generation, which is still beyond the capacity of computational study and needs the guide by experiments [127]. Moreover, current DFT calculations lack the computational power to describe the interactions between a large number of molecules and large-size catalyst particles that reflect the real reaction environment. However, there are some methods available to address this issue, for example, the QM/MM (quantum mechanics/molecular mechanics) method [128]. In this method, the QM region of the system where chemical process occurs is solved by quantum mechanics theory such as DFT and semi-empirical method, while the rest of the system is described by a molecular mechanics force field [129]. Since the QM/MM method combines the accuracy of QM and the speed of MM method, it can handle systems close to real reaction environments with thousands of atoms, especially in enzymatic catalysis. For instance, Lai et al. reported a computational study of the amyloid- β peptide degradation by insulin degrading enzyme (IDE) based on QM/MM with more than 100 thousand of atoms and revealed a four-step mechanism for this process, providing the basis for future study of IDE in humans [130].

4. Outlook of Future Research Direction

Knowing that heterogeneous catalysis is a complicated dynamic process in which chemical species undergo a series of transient reaction steps on catalyst surface through interacting with the active sites, the identification and study of active sites would be very challenging without the use of a comprehensive set of in situ surface characterization techniques. Using the conventional ex situ characterizations like TEM, the surface atoms we observe are sometimes not the real form of active sites because restructuring, segregation and transformation phenomena of the active sites are common when they leave the reactive atmosphere. Despite the enormous potential of in situ TEM/STEM characterizations, there are still technological limitations and disadvantages associated with these techniques and awaiting solutions with continuous research efforts. For instance, recent efforts have been made to develop low-voltage TEM/STEM operating at 20 kV to 80 kV to mitigate the electron beam effects on catalyst materials, with the loss in resolution due to use of low energy electrons being compensated by a smaller Cs through aberration corrections [131,132]. Given this strategy being proven effective, in situ electron microscopy operating at low voltage could represent one future direction in the active site study. Another possible direction is the development of appropriate techniques that could characterize the active site in real in situ conditions and in the meantime analyze the reactants and products on line. In general, techniques that allow the handling of catalysts in real reaction conditions with a dynamic and simultaneous observation of active site evolution are highly desirable in active site study. Besides the techniques, the design of novel active sites for metal and metal oxide-based catalysts, especially for noble-metal-free catalysts with low cost and satisfactory performance, remains an important challenge. For instance, Rh-based catalysts used to be among the most effective catalysts for the decomposition of nitrous oxide, however, satisfactory activity could also be achieved by some metal oxides, hexaaluminates, and perovskites by careful design of the active sites [133]. It's also worth noted that the structure and morphology of the active sites may have significant effects on the catalytic performance. It's expected that one can achieve better activity of the catalysts by modifying the morphology of the active sites. For instance, Li et al. summarized the state-of-art progress of the metal nanoparticle supported by metal oxide core/yolk-shell nanostructures, which showed unique collective and synergetic effects over conventional structures in various catalytic process [134].

With the development of electronic structure theory and computational methods, the computational catalysis approach holds great promise in active site study. The examples discussed in this review all refer to the active sites on transition metals and metal oxides by calculating the

binding energy between the adsorbed molecules and the surface atoms. However, the interactions between the nanoparticles and the support, which could involve support defects and molecule or atom migration, are often more complicated and might play important roles in affecting the active sites. More research efforts are needed to find out how we can systematically and directly include the support effects in the simulations. Some newly discovered theories may be further developed to better simulate the complicated process. For instance, Shen et al. reported the description of adsorption energy on transition metals by considering both ionic bonding and covalent bonding contributions and introduced work function as one additional responsible parameter, with which the adsorption energy on transition metals was more accurately described [135]. This theory may be further extended to other types of catalysts like metal oxides, which requires more work for validation. Moreover, the activity and selectivity properties of active sites in many catalytic processes have been able to be simulated with DFT calculations. In the meantime, more computational approaches need to be developed to simulate some other equally important properties, for instance the catalyst stability and the resistance to poisons. In recent years, machine learning has raised increasing interests in the field of computational chemistry, especially in active sites study [136–139]. For instance, Nørskov's group explored the activity of around 583 adsorption sites from 40 different facets of four different bulk composites for CO₂ reduction with a neural-network-based machine learning method and screened some adsorption sites as candidates of active sites for following DFT calculation, which significantly reduced the number of DFT calculations needed [140]. Nevertheless, with the continuous advances in new experimental techniques and computational methods, a combinational use of these advanced approaches will provide an even more powerful tool in future study of active sites and heterogeneous catalysis.

Author Contributions: Y.P. and Z.P. wrote the paper; X.S., L.Y. and A.B. helped with paper preparation and discussion.

Acknowledgments: This work was financially supported by National Science Foundation (No. CHE-1665265).

Conflicts of Interest: The authors declare no conflict of interest.

References

1. Schlögl, R. Heterogeneous catalysis. *Angew. Chem. Int. Ed.* **2015**, *54*, 3465–3520. [[CrossRef](#)] [[PubMed](#)]
2. George, S.M. Introduction: Heterogeneous catalysis. *Chem. Rev.* **1995**, *95*, 475–476. [[CrossRef](#)]
3. Erisman, J.W.; Sutton, M.A.; Galloway, J.; Klimont, Z.; Winiwarter, W. How a century of ammonia synthesis changed the world. *Nat. Geosci.* **2008**, *1*, 636. [[CrossRef](#)]
4. Schlögl, R. Catalytic Synthesis of Ammonia—A “Never-Ending Story”? *Angew. Chem. Int. Ed.* **2003**, *42*, 2004–2008. [[CrossRef](#)] [[PubMed](#)]
5. Spencer, N.; Schoonmaker, R.; Somorjai, G. Iron single crystals as ammonia synthesis catalysts: Effect of surface structure on catalyst activity. *J. Catal.* **1982**, *74*, 129–135. [[CrossRef](#)]
6. Fu, Q.; Saltsburg, H.; Flytzani-Stephanopoulos, M. Active nonmetallic Au and Pt species on ceria-based water-gas shift catalysts. *Science* **2003**, *301*, 935–938. [[CrossRef](#)] [[PubMed](#)]
7. Li, Y.; Fu, Q.; Flytzani-Stephanopoulos, M. Low-temperature water-gas shift reaction over Cu- and Ni-loaded cerium oxide catalysts. *Appl. Catal. B Environ.* **2000**, *27*, 179–191. [[CrossRef](#)]
8. Hecht, E.S.; Gupta, G.K.; Zhu, H.; Dean, A.M.; Kee, R.J.; Maier, L.; Deutschmann, O. Methane reforming kinetics within a Ni-YSZ SOFC anode support. *Appl. Catal. A Gen.* **2005**, *295*, 40–51. [[CrossRef](#)]
9. Dong, W.-S.; Roh, H.-S.; Jun, K.-W.; Park, S.-E.; Oh, Y.-S. Methane reforming over Ni/Ce-ZrO₂ catalysts: Effect of nickel content. *Appl. Catal. A Gen.* **2002**, *226*, 63–72. [[CrossRef](#)]
10. Laosiripojana, N.; Sutthisripok, W.; Assabumrungrat, S. Synthesis gas production from dry reforming of methane over CeO₂ doped Ni/Al₂O₃: Influence of the doping ceria on the resistance toward carbon formation. *Chem. Eng. J.* **2005**, *112*, 13–22. [[CrossRef](#)]
11. Leitner, W. Carbon dioxide as a raw material: The synthesis of formic acid and its derivatives from CO₂. *Angew. Chem. Int. Ed. Engl.* **1995**, *34*, 2207–2221. [[CrossRef](#)]
12. Preti, D.; Resta, C.; Squarzialupi, S.; Fachinetti, G. Carbon dioxide hydrogenation to formic acid by using a heterogeneous gold catalyst. *Angew. Chem. Int. Ed.* **2011**, *50*, 12551–12554. [[CrossRef](#)] [[PubMed](#)]

13. Peng, G.; Sibener, S.; Schatz, G.C.; Ceyer, S.T.; Mavrikakis, M. CO₂ hydrogenation to formic acid on Ni(111). *J. Phys. Chem. C* **2012**, *116*, 3001–3006. [[CrossRef](#)]
14. Wang, W.-H.; Himeda, Y.; Muckerman, J.T.; Manbeck, G.F.; Fujita, E. CO₂ hydrogenation to formate and methanol as an alternative to photo-and electrochemical CO₂ reduction. *Chem. Rev.* **2015**, *115*, 12936–12973. [[CrossRef](#)] [[PubMed](#)]
15. Bartholomew, C.H.; Farrauto, R.J. *Fundamentals of Industrial Catalytic Processes*; John Wiley & Sons: Hoboken, NJ, USA, 2011.
16. Valden, M.; Lai, X.; Goodman, D.W. Onset of catalytic activity of gold clusters on Titania with the appearance of nonmetallic properties. *Science* **1998**, *281*, 1647–1650. [[CrossRef](#)] [[PubMed](#)]
17. Chen, K.; Bell, A.T.; Iglesia, E. The relationship between the electronic and redox properties of dispersed metal oxides and their turnover rates in oxidative dehydrogenation reactions. *J. Catal.* **2002**, *209*, 35–42. [[CrossRef](#)]
18. Singha, R.K.; Shukla, A.; Yadav, A.; Konathala, L.S.; Bal, R. Effect of metal-support interaction on activity and stability of Ni-CeO₂ catalyst for partial oxidation of methane. *Appl. Catal. B Environ.* **2017**, *202*, 473–488. [[CrossRef](#)]
19. Taylor, H.S. A theory of the catalytic surface. *Proc. R. Soc. Lond. A* **1925**, *108*, 105–111. [[CrossRef](#)]
20. Crampton, A.S.; Rötzer, M.D.; Ridge, C.J.; Yoon, B.; Schweinberger, F.F.; Landman, U.; Heiz, U. Assessing the concept of structure sensitivity or insensitivity for sub-nanometer catalyst materials. *Surf. Sci.* **2016**, *652*, 7–19. [[CrossRef](#)]
21. Balandin, A. The theory of heterogeneous catalytic reactions. The Multiplet hypothesis. Model for dehydrogenation catalysis. *Z. Phys. Chem. Abt. B* **1929**, *2*, 289–316.
22. Balandin, A. Modern State of the Multiplet Theory of Heterogeneous Catalysis. *Adv. Catal.* **1969**, *19*, 1.
23. Boudart, M. Catalysis by supported metals. In *Advances in Catalysis*; Elsevier: Amsterdam, The Netherlands, 1969; Volume 20, pp. 153–166.
24. Cremer, P.S.; Somorjai, G.A. Surface science and catalysis of ethylene hydrogenation. *J. Chem. Soc. Faraday Trans.* **1995**, *91*, 3671–3677. [[CrossRef](#)]
25. Cremer, P.S.; Su, X.; Shen, Y.R.; Somorjai, G.A. Ethylene hydrogenation on Pt (111) monitored in situ at high pressures using sum frequency generation. *J. Am. Chem. Soc.* **1996**, *118*, 2942–2949. [[CrossRef](#)]
26. Somorjai, G.; Zaera, F. Heterogeneous catalysis on the molecular scale. *J. Phys. Chem.* **1982**, *86*, 3070–3078. [[CrossRef](#)]
27. Gillespie, W.; Herz, R.; Petersen, E.; Somorjai, G. The structure sensitivity of n-heptane dehydrocyclization and hydrogenolysis catalyzed by platinum single crystals at atmospheric pressure. *J. Catal.* **1981**, *70*, 147–159. [[CrossRef](#)]
28. Zaera, F. Probing catalytic reactions at surfaces. *Prog. Surf. Sci.* **2001**, *69*, 1–98. [[CrossRef](#)]
29. Nørskov, J.K.; Bligaard, T.; Hvolbæk, B.; Abild-Pedersen, F.; Chorkendorff, I.; Christensen, C.H. The nature of the active site in heterogeneous metal catalysis. *Chem. Soc. Rev.* **2008**, *37*, 2163–2171. [[CrossRef](#)] [[PubMed](#)]
30. Blakely, D.; Somorjai, G. The dehydrogenation and hydrogenolysis of cyclohexane and cyclohexene on stepped (high miller index) platinum surfaces. *J. Catal.* **1976**, *42*, 181–196. [[CrossRef](#)]
31. Yates, J.T., Jr. Surface chemistry at metallic step defect sites. *J. Vac. Sci. Technol. A Vac. Surf. Films* **1995**, *13*, 1359–1367. [[CrossRef](#)]
32. Idriss, H.; Barteau, M.A. Active sites on oxides: From single crystals to catalysts. In *Advances in Catalysis*; Elsevier: Amsterdam, The Netherlands, 2000; Volume 45, pp. 261–331.
33. Somorjai, G. Active sites in heterogeneous catalysis. In *Advances in Catalysis*; Elsevier: Amsterdam, The Netherlands, 1977; Volume 26, pp. 1–68.
34. Deutschmann, O.; Knözinger, H.; Kochloefl, K.; Turek, T. Heterogeneous catalysis and solid catalysts. *Ullmann's Encycl. Ind. Chem.* **2009**. [[CrossRef](#)]
35. Mars, P.; Van Krevelen, D.W. Oxidations carried out by means of vanadium oxide catalysts. *Chem. Eng. Sci.* **1954**, *3*, 41–59. [[CrossRef](#)]
36. Schubert, M.; Kahlich, M.; Gasteiger, H.; Behm, R. Correlation between CO surface coverage and selectivity/kinetics for the preferential CO oxidation over Pt/ γ -Al₂O₃ and Au/ α -Fe₂O₃: An in-situ DRIFTS study. *J. Power Sources* **1999**, *84*, 175–182. [[CrossRef](#)]
37. Qiao, B.; Wang, A.; Li, L.; Lin, Q.; Wei, H.; Liu, J.; Zhang, T. Ferric oxide-supported Pt subnano clusters for preferential oxidation of CO in H₂-rich gas at room temperature. *ACS Catal.* **2014**, *4*, 2113–2117. [[CrossRef](#)]

38. Takanabe, K.; Nagaoka, K.; Nariai, K.; Aika, K.-I. Titania-supported cobalt and nickel bimetallic catalysts for carbon dioxide reforming of methane. *J. Catal.* **2005**, *232*, 268–275. [[CrossRef](#)]
39. Zhang, J.; Wang, H.; Dalai, A.K. Development of stable bimetallic catalysts for carbon dioxide reforming of methane. *J. Catal.* **2007**, *249*, 300–310. [[CrossRef](#)]
40. San-José-Alonso, D.; Juan-Juan, J.; Illán-Gómez, M.; Román-Martínez, M. Ni, Co and bimetallic Ni-Co catalysts for the dry reforming of methane. *Appl. Catal. A Gen.* **2009**, *371*, 54–59. [[CrossRef](#)]
41. Steinhauer, B.; Kasireddy, M.R.; Radnik, J.; Martin, A. Development of Ni-Pd bimetallic catalysts for the utilization of carbon dioxide and methane by dry reforming. *Appl. Catal. A Gen.* **2009**, *366*, 333–341. [[CrossRef](#)]
42. Tsyganok, A.I.; Inaba, M.; Tsunoda, T.; Uchida, K.; Suzuki, K.; Takehira, K.; Hayakawa, T. Rational design of Mg-Al mixed oxide-supported bimetallic catalysts for dry reforming of methane. *Appl. Catal. A Gen.* **2005**, *292*, 328–343. [[CrossRef](#)]
43. Navarro, R.; Pawelec, B.; Trejo, J.; Mariscal, R.; Fierro, J. Hydrogenation of aromatics on sulfur-resistant PtPd bimetallic catalysts. *J. Catal.* **2000**, *189*, 184–194. [[CrossRef](#)]
44. Hwang, S.Y.; Zhang, C.; Yurchekfrod, E.; Peng, Z. Property of Pt-Ag Alloy Nanoparticle Catalysts in Carbon Monoxide Oxidation. *J. Phys. Chem. C* **2014**, *118*, 28739–28745. [[CrossRef](#)]
45. Pan, Y.; Hwang, S.Y.; Shen, X.; Yang, J.; Zeng, J.; Wu, M.; Peng, Z. Computation-Guided Development of Platinum Alloy Catalyst for Carbon Monoxide Preferential Oxidation. *ACS Catal.* **2018**, *8*, 5777–5786. [[CrossRef](#)]
46. Ko, E.Y.; Park, E.D.; Lee, H.C.; Lee, D.; Kim, S. Supported Pt-Co Catalysts for Selective CO Oxidation in a Hydrogen-Rich Stream. *Angew. Chem. Int. Ed.* **2007**, *46*, 734–737. [[CrossRef](#)] [[PubMed](#)]
47. Lobera, M.; Téllez, C.; Herguido, J.; Menéndez, M. Catalytic purification of H₂-rich streams by CO-PROX over Pt-Co-Ce/ γ -Al₂O₃ in fluidized bed reactors. *Catal. Today* **2010**, *157*, 404–409. [[CrossRef](#)]
48. Chorkendorff, I.; Niemantsverdriet, J.W. *Concepts of Modern Catalysis and Kinetics*; John Wiley & Sons: Hoboken, NJ, USA, 2017.
49. Hwang, S.Y.; Yurchekfrod, E.; Zhang, C.; Peng, Z. Low-Temperature Preferential Oxidation of Carbon Monoxide on Pt₃Ni Alloy Nanoparticle Catalyst with Engineered Surface. *ChemCatChem* **2016**, *8*, 97–101. [[CrossRef](#)]
50. Ko, E.-Y.; Park, E.D.; Seo, K.W.; Lee, H.C.; Lee, D.; Kim, S. A comparative study of catalysts for the preferential CO oxidation in excess hydrogen. *Catal. Today* **2006**, *116*, 377–383. [[CrossRef](#)]
51. Gupta, P.; Paul, S. Solid acids: Green alternatives for acid catalysis. *Catal. Today* **2014**, *236*, 153–170. [[CrossRef](#)]
52. Phung, T.K.; Busca, G. Diethyl ether cracking and ethanol dehydration: Acid catalysis and reaction paths. *Chem. Eng. J.* **2015**, *272*, 92–101. [[CrossRef](#)]
53. Li, H.; Fang, Z.; Luo, J.; Yang, S. Direct conversion of biomass components to the biofuel methyl levulinate catalyzed by acid-base bifunctional zirconia-zeolites. *Appl. Catal. B Environ.* **2017**, *200*, 182–191. [[CrossRef](#)]
54. Saravanan, K.; Tyagi, B.; Shukla, R.S.; Bajaj, H. Esterification of palmitic acid with methanol over template-assisted mesoporous sulfated zirconia solid acid catalyst. *Appl. Catal. B Environ.* **2015**, *172*, 108–115. [[CrossRef](#)]
55. Sani, Y.M.; Daud, W.M.A.W.; Aziz, A.A. Activity of solid acid catalysts for biodiesel production: A critical review. *Appl. Catal. A Gen.* **2014**, *470*, 140–161. [[CrossRef](#)]
56. Takahara, I.; Saito, M.; Inaba, M.; Murata, K. Dehydration of ethanol into ethylene over solid acid catalysts. *Catal. Lett.* **2005**, *105*, 249–252. [[CrossRef](#)]
57. Corma, A.; Planelles, J.; Sanchez-Marin, J.; Tomas, F. The role of different types of acid site in the cracking of alkanes on zeolite catalysts. *J. Catal.* **1985**, *93*, 30–37. [[CrossRef](#)]
58. Tang, B.; Dai, W.; Wu, G.; Guan, N.; Li, L.; Hunger, M. Improved postsynthesis strategy to Sn-Beta zeolites as Lewis acid catalysts for the ring-opening hydration of epoxides. *ACS Catal.* **2014**, *4*, 2801–2810. [[CrossRef](#)]
59. Alaerts, L.; Séguin, E.; Poelman, H.; Thibault-Starzyk, F.; Jacobs, P.A.; De Vos, D.E. Probing the Lewis Acidity and Catalytic Activity of the Metal-Organic Framework [Cu₃(btc)₂] (BTC = Benzene-1, 3, 5-tricarboxylate). *Chem. Eur. J.* **2006**, *12*, 7353–7363. [[CrossRef](#)] [[PubMed](#)]
60. Che, M.; Védrine, J.C. *Characterization of Solid Materials and Heterogeneous Catalysts: From Structure to Surface Reactivity*; John Wiley & Sons: Hoboken, NJ, USA, 2012.
61. Leofanti, G.; Padovan, M.; Tozzola, G.; Venturelli, B. Surface area and pore texture of catalysts. *Catal. Today* **1998**, *41*, 207–219. [[CrossRef](#)]

62. Jona, F.; Strozier, J., Jr.; Yang, W. Low-energy electron diffraction for surface structure analysis. *Rep. Prog. Phys.* **1982**, *45*, 527. [[CrossRef](#)]
63. Yin, C.; Negreiros, F.R.; Barcaro, G.; Beniya, A.; Sementa, L.; Tyo, E.C.; Bartling, S.; Meiwes-Broer, K.-H.; Seifert, S.; Hirata, H. Alumina-supported sub-nanometer Pt 10 clusters: Amorphization and role of the support material in a highly active CO oxidation catalyst. *J. Mater. Chem. A* **2017**, *5*, 4923–4931. [[CrossRef](#)]
64. Hollander, J.M.; Jolly, W.L. X-ray photoelectron spectroscopy. *Acc. Chem. Res.* **1970**, *3*, 193–200. [[CrossRef](#)]
65. Zhang, C.; Oliaee, S.N.; Hwang, S.Y.; Kong, X.; Peng, Z. A Generic Wet Impregnation Method for Preparing Substrate-Supported Platinum Group Metal and Alloy Nanoparticles with Controlled Particle Morphology. *Nano Lett.* **2015**, *16*, 164–169. [[CrossRef](#)] [[PubMed](#)]
66. Chang, C.C. Auger electron spectroscopy. *Surf. Sci.* **1971**, *25*, 53–79. [[CrossRef](#)]
67. Yan, T.; Redman, D.W.; Yu, W.-Y.; Flaherty, D.W.; Rodriguez, J.A.; Mullins, C.B. CO oxidation on inverse Fe₂O₃/Au (1 1 1) model catalysts. *J. Catal.* **2012**, *294*, 216–222. [[CrossRef](#)]
68. Binnig, G.; Rohrer, H. Scanning tunneling microscopy. *Surf. Sci.* **1983**, *126*, 236–244. [[CrossRef](#)]
69. Zhao, G.; Yang, F.; Chen, Z.; Liu, Q.; Ji, Y.; Zhang, Y.; Niu, Z.; Mao, J.; Bao, X.; Hu, P. Metal/oxide interfacial effects on the selective oxidation of primary alcohols. *Nat. Commun.* **2017**, *8*, 14039. [[CrossRef](#)] [[PubMed](#)]
70. Ali, A.; Henda, R.; Aluha, J.; Abatzoglou, N. Co-doped ZnO thin films grown by pulsed electron beam ablation as model nano-catalysts in fischer-tropsch synthesis. *AIChE J.* **2018**. [[CrossRef](#)]
71. Niehus, H.; Heiland, W.; Taglauer, E. Low-energy ion scattering at surfaces. *Surf. Sci. Rep.* **1993**, *17*, 213–303. [[CrossRef](#)]
72. Yang, Z.; Chen, W.; Zheng, J.; Yang, Z.; Zhang, N.; Zhong, C.-J.; Chen, B.H. Efficient low-temperature hydrogenation of acetone on bimetallic Pt-Ru/C catalyst. *J. Catal.* **2018**, *363*, 52–62. [[CrossRef](#)]
73. Colthup, N. *Introduction to Infrared and Raman Spectroscopy*; Elsevier: Amsterdam, The Netherlands, 2012.
74. Stuart, B. Infrared spectroscopy. *Kirk-Othmer Encycl. Chem. Technol.* **2005**. [[CrossRef](#)]
75. Otake, K.-I.; Cui, Y.; Buru, C.T.; Li, Z.; Hupp, J.T.; Farha, O.K. Single-Atom-Based Vanadium Oxide Catalysts Supported on Metal-Organic Frameworks: Selective Alcohol Oxidation and Structure-Activity Relationship. *J. Am. Chem. Soc.* **2018**, *140*, 8652–8656. [[CrossRef](#)] [[PubMed](#)]
76. Perkampus, H.-H. *UV-VIS Spectroscopy and its Applications*; Springer Science & Business Media: Berlin, Germany, 2013.
77. Swinehart, D. The beer-lambert law. *J. Chem. Educ.* **1962**, *39*, 333. [[CrossRef](#)]
78. Goetze, J.; Meirer, F.; Yarulina, I.; Gascon, J.; Kapteijn, F.; Ruiz-Martínez, J.; Weckhuysen, B.M. Insights into the activity and deactivation of the methanol-to-olefins process over different small-pore zeolites as studied with operando UV-vis spectroscopy. *ACS Catal.* **2017**, *7*, 4033–4046. [[CrossRef](#)] [[PubMed](#)]
79. Yano, J.; Yachandra, V.K. X-ray absorption spectroscopy. *Photosynth. Res.* **2009**, *102*, 241. [[CrossRef](#)] [[PubMed](#)]
80. Magadzu, T.; Yang, J.; Henao, J.; Kung, M.; Kung, H.; Scurrell, M. Low-temperature water-gas shift reaction over Au supported on anatase in the presence of copper: EXAFS/XANES analysis of gold-copper ion mixtures on TiO₂. *J. Phys. Chem. C* **2017**, *121*, 8812–8823. [[CrossRef](#)]
81. Warren, B.E. *X-Ray Diffraction*; Courier Corporation: Chelmsford, MA, USA, 1990.
82. Mebrahtu, C.; Abate, S.; Perathoner, S.; Chen, S.; Centi, G. CO₂ methanation over Ni catalysts based on ternary and quaternary mixed oxide: A comparison and analysis of the structure-activity relationships. *Catal. Today* **2018**, *304*, 181–189. [[CrossRef](#)]
83. Williams, D.B.; Carter, C.B. The transmission electron microscope. In *Transmission Electron Microscopy*; Springer: Cham, Switzerland, 1996; pp. 3–17.
84. Goldstein, J.I.; Newbury, D.E.; Michael, J.R.; Ritchie, N.W.; Scott, J.H.J.; Joy, D.C. *Scanning Electron Microscopy and X-Ray Microanalysis*; Springer: Cham, Switzerland, 2017.
85. Xu, K.; Chen, P.; Li, X.; Tong, Y.; Ding, H.; Wu, X.; Chu, W.; Peng, Z.; Wu, C.; Xie, Y. Metallic nickel nitride nanosheets realizing enhanced electrochemical water oxidation. *J. Am. Chem. Soc.* **2015**, *137*, 4119–4125. [[CrossRef](#)] [[PubMed](#)]
86. Nørskov, J.K.; Bligaard, T.; Rossmeisl, J.; Christensen, C.H. Towards the computational design of solid catalysts. *Nat. Chem.* **2009**, *1*, 37. [[CrossRef](#)] [[PubMed](#)]
87. Woodward, R.B.; Hoffmann, R. The conservation of orbital symmetry. *Angew. Chem. Int. Ed. Engl.* **1969**, *8*, 781–853. [[CrossRef](#)]
88. Hoffmann, R. Interaction of orbitals through space and through bonds. *Acc. Chem. Res.* **1971**, *4*, 1–9. [[CrossRef](#)]

89. Ammeter, J.; Bürgi, H.; Thibeault, J.; Hoffmann, R. Counterintuitive orbital mixing in semiempirical and ab initio molecular orbital calculations. *J. Am. Chem. Soc.* **1978**, *100*, 3686–3692. [[CrossRef](#)]
90. Hoffmann, R. An extended Hückel theory. I. hydrocarbons. *J. Chem. Phys.* **1963**, *39*, 1397–1412. [[CrossRef](#)]
91. Gomez-Jeria, J.S. The limits of the Extended Hückel Theory to Calculate the Total Density of States of Medium-Sized Molecules. *J. Chil. Chem. Soc.* **2006**, *51*, 1061–1064. [[CrossRef](#)]
92. Anderson, A.B.; Hoffmann, R. Description of diatomic molecules using one electron configuration energies with two-body interactions. *J. Chem. Phys.* **1974**, *60*, 4271–4273. [[CrossRef](#)]
93. Anderson, A.B. Derivation of the extended Hückel method with corrections: One electron molecular orbital theory for energy level and structure determinations. *J. Chem. Phys.* **1975**, *62*, 1187–1188. [[CrossRef](#)]
94. Anderson, A.B.; Grimes, R.W.; Hong, S.Y. Toward a better understanding of the atom superposition and electron delocalization molecular orbital theory and a systematic test: Diatomic oxides of the first transition-metal series, bonding and trends. *J. Phys. Chem.* **1987**, *91*, 4245–4250. [[CrossRef](#)]
95. De Koster, A.; Van Santen, R. Molecular orbital studies of the adsorption of CH₃, CH₂, and CH on Rh(111) and Ni(111) surfaces. *J. Catal.* **1991**, *127*, 141–166. [[CrossRef](#)]
96. VAN SANTEN, R.A.; NEUROCK, M. Concepts in theoretical heterogeneous catalytic reactivity. *Catal. Rev.* **1995**, *37*, 557–698. [[CrossRef](#)]
97. Vedrine, J.C. Revisiting active sites in heterogeneous catalysis: Their structure and their dynamic behaviour. *Appl. Catal. A Gen.* **2014**, *474*, 40–50. [[CrossRef](#)]
98. Slater, J.C. A simplification of the Hartree-Fock method. *Phys. Rev.* **1951**, *81*, 385. [[CrossRef](#)]
99. Radhakrishnan, R.; Oyama, S.T.; Ohminami, Y.; Asakura, K. Structure of MnO_x/Al₂O₃ Catalyst: A Study Using EXAFS, In Situ Laser Raman Spectroscopy and ab Initio Calculations. *J. Phys. Chem. B* **2001**, *105*, 9067–9070. [[CrossRef](#)]
100. Thomas, L.H. The Calculation of Atomic Fields. *Math. Proc. Camb. Philos. Soc.* **1927**, *23*, 542–548. [[CrossRef](#)]
101. Hohenberg, P.; Kohn, W. Inhomogeneous electron gas. *Phys. Rev.* **1964**, *136*, B864. [[CrossRef](#)]
102. Behrens, M.; Studt, F.; Kasatkin, I.; Kühl, S.; Hävecker, M.; Abild-Pedersen, F.; Zander, S.; Girgsdies, F.; Kurr, P.; Knief, B.-L. The active site of methanol synthesis over Cu/ZnO/Al₂O₃ industrial catalysts. *Science* **2012**, 1219831. [[CrossRef](#)] [[PubMed](#)]
103. Robertson, A.W.; Lee, G.-D.; He, K.; Fan, Y.; Allen, C.S.; Lee, S.; Kim, H.; Yoon, E.; Zheng, H.; Kirkland, A.I. Partial dislocations in graphene and their atomic level migration dynamics. *Nano Lett.* **2015**, *15*, 5950–5955. [[CrossRef](#)] [[PubMed](#)]
104. Huang, J.Y.; Zhong, L.; Wang, C.M.; Sullivan, J.P.; Xu, W.; Zhang, L.Q.; Mao, S.X.; Hudak, N.S.; Liu, X.H.; Subramanian, A. In situ observation of the electrochemical lithiation of a single SnO₂ nanowire electrode. *Science* **2010**, *330*, 1515–1520. [[CrossRef](#)] [[PubMed](#)]
105. Liao, H.-G.; Zherebetsky, D.; Xin, H.; Czarnik, C.; Ercius, P.; Elmlund, H.; Pan, M.; Wang, L.-W.; Zheng, H. Facet development during platinum nanocube growth. *Science* **2014**, *345*, 916–919. [[CrossRef](#)] [[PubMed](#)]
106. Vendelbo, S.; Elkjær, C.; Falsig, H.; Puspitasari, I.; Dona, P.; Mele, L.; Morana, B.; Nelissen, B.; Van Rijn, R.; Creemer, J. Visualization of oscillatory behaviour of Pt nanoparticles catalysing CO oxidation. *Nat. Mater.* **2014**, *13*, 884. [[CrossRef](#)] [[PubMed](#)]
107. Niu, K.-Y.; Liu, M.; Persson, K.A.; Han, Y.; Zheng, H. Strain-Mediated Interfacial Dynamics during Au–PbS Core–Shell Nanostructure Formation. *ACS Nano* **2016**, *10*, 6235–6240. [[CrossRef](#)] [[PubMed](#)]
108. Shen, X.; Dai, S.; Zhang, C.; Zhang, S.; Sharkey, S.M.; Graham, G.W.; Pan, X.; Peng, Z. In situ atomic-scale observation of the two-dimensional Co (OH)₂ transition at atmospheric pressure. *Chem. Mater.* **2017**, *29*, 4572–4579. [[CrossRef](#)]
109. Hammer, B.; Nørskov, J. Electronic factors determining the reactivity of metal surfaces. *Surf. Sci.* **1995**, *343*, 211–220. [[CrossRef](#)]
110. Hammer, B.; Nørskov, J.K. Theoretical surface science and catalysis—Calculations and concepts. In *Advances in Catalysis*; Elsevier: Cham, Switzerland, 2000; Volume 45, pp. 71–129.
111. Studt, F.; Abild-Pedersen, F.; Bligaard, T.; Sørensen, R.Z.; Christensen, C.H.; Nørskov, J.K. Identification of non-precious metal alloy catalysts for selective hydrogenation of acetylene. *Science* **2008**, *320*, 1320–1322. [[CrossRef](#)] [[PubMed](#)]
112. Abild-Pedersen, F.; Greeley, J.; Studt, F.; Rossmeisl, J.; Munter, T.; Moses, P.G.; Skulason, E.; Bligaard, T.; Nørskov, J.K. Scaling properties of adsorption energies for hydrogen-containing molecules on transition-metal surfaces. *Phys. Rev. Lett.* **2007**, *99*, 016105. [[CrossRef](#)] [[PubMed](#)]

113. Vojvodic, A.; Hellman, A.; Ruberto, C.; Lundqvist, B.I. From electronic structure to catalytic activity: A single descriptor for adsorption and reactivity on transition-metal carbides. *Phys. Rev. Lett.* **2009**, *103*, 146103. [[CrossRef](#)] [[PubMed](#)]
114. Fernández, E.M.; Moses, P.G.; Toftelund, A.; Hansen, H.A.; Martínez, J.I.; Abild-Pedersen, F.; Kleis, J.; Hinnemann, B.; Rossmeisl, J.; Bligaard, T. Scaling relationships for adsorption energies on transition metal oxide, sulfide, and nitride surfaces. *Angew. Chem. Int. Ed.* **2008**, *47*, 4683–4686. [[CrossRef](#)] [[PubMed](#)]
115. Fu, Q.; Cao, X.; Luo, Y. Identification of the scaling relations for binary noble-metal nanoparticles. *J. Phys. Chem. C* **2013**, *117*, 2849–2854. [[CrossRef](#)]
116. Su, D.S.; Zhang, B.; Schlögl, R. Electron Microscopy of Solid Catalysts Transforming from a Challenge to a Toolbox. *Chem. Rev.* **2015**, *115*, 2818–2882. [[CrossRef](#)] [[PubMed](#)]
117. Amakawa, K.; Wrabetz, S.; Kröhnert, J.; Tzolova-Müller, G.; Schlögl, R.; Trunschke, A. In situ generation of active sites in olefin metathesis. *J. Am. Chem. Soc.* **2012**, *134*, 11462–11473. [[CrossRef](#)] [[PubMed](#)]
118. Pantazidis, A.; Burrows, A.; Kiely, C.; Mirodatos, C. Direct evidence of active surface reconstruction during oxidative dehydrogenation of propane over VMgO catalyst. *J. Catal.* **1998**, *177*, 325–334. [[CrossRef](#)]
119. Zhang, B.; Wang, D.; Zhang, W.; Su, D.S.; Schlögl, R. Structural Dynamics of Low-Symmetry Au Nanoparticles Stimulated by Electron Irradiation. *Chem. Eur. J.* **2011**, *17*, 12877–12881. [[CrossRef](#)] [[PubMed](#)]
120. Wieske, M.; Su, D.S.; Beckmann, F.; Schlögl, R. Electron-Beam-Induced Structural Variations of Divanadium Pentoxide (V₂O₅) at Liquid Helium Temperature. *Catal. Lett.* **2002**, *81*, 43–47. [[CrossRef](#)]
121. Su, D.S.; Wieske, M.; Beckmann, E.; Blume, A.; Mestl, G.; Schlögl, R. Electron beam induced reduction of V₂O₅ studied by analytical electron microscopy. *Catal. Lett.* **2001**, *75*, 81–86. [[CrossRef](#)]
122. Ulissi, Z.W.; Medford, A.J.; Bligaard, T.; Nørskov, J.K. To address surface reaction network complexity using scaling relations machine learning and DFT calculations. *Nat. Commun.* **2017**, *8*, 14621. [[CrossRef](#)] [[PubMed](#)]
123. Hinuma, Y.; Hayashi, H.; Kumagai, Y.; Tanaka, I.; Oba, F. Comparison of approximations in density functional theory calculations: Energetics and structure of binary oxides. *Phys. Rev. B* **2017**, *96*, 094102. [[CrossRef](#)]
124. Kohan, A.; Ceder, G.; Morgan, D.; Van de Walle, C.G. First-principles study of native point defects in ZnO. *Phys. Rev. B* **2000**, *61*, 15019. [[CrossRef](#)]
125. Solans-Monfort, X.; Branchadell, V.; Sodupe, M.; Sierka, M.; Sauer, J. Electron hole formation in acidic zeolite catalysts. *J. Chem. Phys.* **2004**, *121*, 6034–6041. [[CrossRef](#)] [[PubMed](#)]
126. Chrétien, S.; Metiu, H. O₂ evolution on a clean partially reduced rutile TiO₂(110) surface and on the same surface precovered with Au₁ and Au₂: The importance of spin conservation. *J. Chem. Phys.* **2008**, *129*, 074705. [[CrossRef](#)] [[PubMed](#)]
127. Jain, A.; Shin, Y.; Persson, K.A. Computational predictions of energy materials using density functional theory. *Nat. Rev. Mater.* **2016**, *1*, 15004. [[CrossRef](#)]
128. Senn, H.M.; Thiel, W. QM/MM methods for biomolecular systems. *Angew. Chem. Int. Ed.* **2009**, *48*, 1198–1229. [[CrossRef](#)] [[PubMed](#)]
129. Lin, H.; Truhlar, D.G. QM/MM: What have we learned, where are we, and where do we go from here? *Theor. Chem. Acc.* **2007**, *117*, 185. [[CrossRef](#)]
130. Lai, R.; Tang, W.-J.; Li, H. Catalytic Mechanism of Amyloid-β Peptide Degradation by Insulin Degrading Enzyme: Insights from Quantum Mechanics and Molecular Mechanics Style Møller–Plesset Second Order Perturbation Theory Calculation. *J. Chem. Inf. Model.* **2018**, *58*, 1926–1934. [[CrossRef](#)] [[PubMed](#)]
131. Kaiser, U.; Biskupek, J.; Meyer, J.; Leschner, J.; Lechner, L.; Rose, H.; Stöger-Pollach, M.; Khlobystov, A.; Hartel, P.; Müller, H. Transmission electron microscopy at 20 kV for imaging and spectroscopy. *Ultramicroscopy* **2011**, *111*, 1239–1246. [[CrossRef](#)] [[PubMed](#)]
132. Bell, D.C.; Russo, C.J.; Kolmykov, D.V. 40 keV atomic resolution TEM. *Ultramicroscopy* **2012**, *114*, 31–37. [[CrossRef](#)] [[PubMed](#)]
133. Konsolakis, M. Recent advances on nitrous oxide (N₂O) decomposition over non-noble-metal oxide catalysts: Catalytic performance, mechanistic considerations, and surface chemistry aspects. *ACS Catal.* **2015**, *5*, 6397–6421. [[CrossRef](#)]
134. Li, G.; Tang, Z. Noble metal nanoparticle@ metal oxide core/yolk-shell nanostructures as catalysts: Recent progress and perspective. *Nanoscale* **2014**, *6*, 3995–4011. [[CrossRef](#)] [[PubMed](#)]
135. Shen, X.; Pan, Y.; Liu, B.; Yang, J.; Zeng, J.; Peng, Z. More accurate depiction of adsorption energy on transition metals using work function as one additional descriptor. *Phys. Chem. Chem. Phys.* **2017**, *19*, 12628–12632. [[CrossRef](#)] [[PubMed](#)]

136. Faber, F.A.; Hutchison, L.; Huang, B.; Gilmer, J.; Schoenholz, S.S.; Dahl, G.E.; Vinyals, O.; Kearnes, S.; Riley, P.F.; von Lilienfeld, O.A. Prediction errors of molecular machine learning models lower than hybrid DFT error. *J. Chem. Theory Comput.* **2017**, *13*, 5255–5264. [[CrossRef](#)] [[PubMed](#)]
137. Deringer, V.L.; Caro, M.A.; Jana, R.; Aarva, A.; Elliott, S.R.; Laurila, T.; Csányi, G.; Pastewka, L. Computational Surface Chemistry of Tetrahedral Amorphous Carbon by Combining Machine Learning and DFT. *Chem. Mater.* **2018**. [[CrossRef](#)]
138. Dragoni, D.; Daff, T.D.; Csányi, G.; Marzari, N. Achieving DFT accuracy with a machine-learning interatomic potential: Thermomechanics and defects in bcc ferromagnetic iron. *Phys. Rev. Mater.* **2018**, *2*, 013808. [[CrossRef](#)]
139. Chmiela, S.; Tkatchenko, A.; Sauceda, H.E.; Poltavsky, I.; Schütt, K.T.; Müller, K.-R. Machine learning of accurate energy-conserving molecular force fields. *Sci. Adv.* **2017**, *3*, e1603015. [[CrossRef](#)] [[PubMed](#)]
140. Ulissi, Z.W.; Tang, M.T.; Xiao, J.; Liu, X.; Torelli, D.A.; Karamad, M.; Cummins, K.; Hahn, C.; Lewis, N.S.; Jaramillo, T.F. Machine-learning methods enable exhaustive searches for active bimetallic facets and reveal active site motifs for CO₂ reduction. *ACS Catal.* **2017**, *7*, 6600–6608. [[CrossRef](#)]



© 2018 by the authors. Licensee MDPI, Basel, Switzerland. This article is an open access article distributed under the terms and conditions of the Creative Commons Attribution (CC BY) license (<http://creativecommons.org/licenses/by/4.0/>).